Nuclear Engineering and Technology 50 (2018) 1068–1078

Contents lists available at ScienceDirect

Nuclear Engineering and Technology

journal homepage: www.elsevier.com/locate/net

Original Article

Experimental study of bubble behaviors and CHF on printed circuit board (PCB) in saturated pool water at various inclination angles

Elvira F. Tanjung, Bernard O. Alunda, Yong Joong Lee, Daeseong Jo*

School of Mechanical Engineering, Kyungpook National University, 80 Daehak-ro, Buk-gu, Daegu, 702-701, Republic of Korea

ARTICLE INFO

Article history:
Received 1 December 2017
Received in revised form
13 March 2018
Accepted 11 June 2018
Available online 15 June 2018

Keywords:
Critical heat flux
Inclination angle
Pool boiling
Bubble behavior

ABSTRACT

Experiments were performed to investigate bubble behaviors and pool boiling Critical Heat Flux (CHF) on a thin flat rectangular copper heater fabricated on Printed Circuit Board (PCB), at various inclination angles. The surface inclination angles were 0°, 45°, 90°, 135°, and 180°. Results showed the Onset of Nucleate Boiling (ONB) heat flux increased with increasing heater orientation from 0° to 90°, while early ONB occurred when the heater faced downwards (135° and 180°). The nucleate boiling was observed to be unstable at low heat flux (1–21% of CHF) and changed into typical boiling when the heat flux was above 21% of CHF. The result shows the CHF decreased with increasing heater orientation from 0° to 180°. In addition, the bubble departure diameter at the heater facing upwards (0°, 45°, and 90°) was more prominent compared to that of the heater facing downward (135°). The nucleation site density also observed increased with increasing heat flux. Moreover, the departed bubbles with larger size were observed to require a longer time to re-heat and activate new nucleation sites. These results proved that the ONB, CHF, and bubble dynamics were strongly dependent on the heater surface orientation.

1. Introduction

Bubble behaviors and Critical Heat Flux (CHF) play essential roles in boiling processes as they are widely used in cooling applications, such as heat exchangers, small electronic devices, and large power plants. Although numerous experimental studies have investigated and predicted the CHF and boiling phenomenon, the results have not been satisfactory. Kwark et al. [1] investigated the effects of pressure, orientation, and heater size on pool boiling of water. They observed a gradual reduction of CHF with increasing the heater size due to bigger heater offered longer resistive to the coolant. Rainey and You [2] investigated the effect of heater size and orientation on pool boiling. They found that for small heaters the CHF was higher compared to the bigger. The similar investigation reported by Lu et al. [3] found that the spreading liquid and the heater size could retard the occurrence of CHF, with the CHF increasing as the heater size reduced. Aside from heater size, heater surface condition also affected the CHF. Heater surface with a high value of roughness represented of large number of cavities on the surface which can be activated and generate bubbles. At the same time, when the bubbles are generated and detached from the surface, the rewetting of the nucleation sites is enhanced which could delay the CHF. Chu et al. [4] experimented to expound the effect of structure surfaces for enhanced pool boiling heat transfer. They postulated, the roughness-magnified surface enhanced the CHF and should be considered as one of the factors that involved in CHF aside of contact angle variation with temperature.

Research of CHF and bubble phenomena in pool boiling has continuously caught the attention of researchers around the world due to the complex boiling phenomena. The effect of heater surface orientation on bubble behaviors and CHF became a fascinated topic of pool boiling. Table 1 presents a summary of the previous studies related to the effects of the heater orientation on CHF. As the reference, the heater with the orientation of the horizontal facing upward is defined as the 0° inclination angle.

Githinji and Sabersky [5] investigated the effects of the heated surface orientation on nucleate boiling. They found that the CHF for the heater facing downward was lower compared to that of the heater facing upward because of the tendency of the bubbles to accumulate and laminate the heated surface, thereby stopping the liquid from accessing the heated surface. Marcus and Dropkin [6] and Nishikawa et al. [7] observed significant effects at a low heat flux as the heater orientation increased. During the 1970s, Vishnev [8] had first formulated the correlation between the pool boiling

* Corresponding author.
E-mail address: djo@knu.ac.kr (D. Jo).

https://doi.org/10.1016/j.net.2018.06.011

Nomenclature

C_{CHF}	Pool boiling CHF coefficient
d_b	Bubble departure diameter
f	Bubble frequency
$f(\theta)$	Influence of the inclination angle
g	Gravitational constant
hfg	Latent heat of evaporation
q''_{CHF}	Critical heat flux
q''_0	Critical heat flux at 0° inclination angle
t_g	Bubble growth time
t_w	Bubble waiting time

Greek symbols

ρ_f	Saturated liquid density
ρ_g	Saturated vapor density
θ	Inclination angle measured from the horizontal facing upward position
σ	Surface tension

CHF and the heater surface orientation based on the experimental data of Lyon [9]. Table 2 presents various correlations of the CHF with the effect of surface orientations. Moreover, Chen [10] postulated that the Rohsenow correlation [11] should add the heater surface orientation as a new parameter because it influenced the nucleate boiling heat transfer significantly.

Guo and El-Genk [12] and El-Genk and Guo [13] investigated the effects of heater orientation in a saturated pool. They observed that the CHF and minimum film boiling heat flux decreased with increasing heater orientation. Moreover, at a low heat flux, the heat transfer rate increased with the increase in the heater orientation. Based on their previous study [12], they developed correlations for different fluids describing the effect of the heater orientation on the pool boiling CHF [13].

Brusstar and Merte [14] developed a model for the CHF in the pool and flow boiling. The model was based on the relationship between the bubble attachment time and the CHF value with the validity limited to the range $90^\circ \leq \theta < 165^\circ$, but it was applied for all heater orientation angles. Chang and You [15], and recently, Arik and Bar-Cohen [16] also developed pool boiling CHF correlations based on their experimental data for FC-72 and NOVEC fluids, respectively. The NOVEC fluids have low global warming potential

Table 1
Previous studies related to heater inclination angle effects in pool boiling CHF.

Reference	Working Fluid	Boiling Surface (width × length) or diameter	Inclination Angles (deg)
Githinji and Sabersky [5]	Isopropyl alcohol	Chromax (3.175 mm × 101.6 mm)	0, 90, and 180
Marcus and Dropkin [6]	Water	Copper (50.8 mm × 50.8 mm)	0, 22.5, 45, 67.5, and 90
Lyon [9]	Helium	Platinum disk, 10 mm of diameter	0, 90, 140, and 180
Vishnev [8]	Helium	Platinum disk, 10 mm of diameter	0, 90, 140, and 180
Chen [10]	Freon-11	Copper (25 mm × 37 mm)	0, 30, 60, 90, 120, 150, 165, and 180
Nishikawa et al. [7]	Water	Copper (42 mm × 175 mm)	0, 90, 120, 150, 165, and 175
Guo and El-Genk [12]	Water	Copper disk, 50.8 mm of diameter	90, 135, 150, 165, 170, 175, and 180
El-Genk and Guo [13]	Water	Copper disk, 50.8 mm of diameter	0, 5, 10, 15, 30, 45, and 90
Brusstar and Merte [14]	R-113	Copper (19.1 mm × 38.1 mm)	0, 30, 90, 120, and 135
Chang and You [15]	FC-72	Copper (10 mm × 10 mm)	0, 45, 90, 135, and 180
Arik and Bar-Cohen [16]	FC-72 and HFE-7100	ATC 2.6 chip package	0 to 180
Rainey and You [2]	FC-72	Copper (20 mm × 20 mm) (50 mm × 50 mm)	0, 45, 90, 135, 160, and 180
Priarone [18]	FC-72 and HFE-7100	Copper (23.5 mm × 30 mm)	0, 45, 90, 135, and 175
Liao et al. [19]	Water	Copper cylinder, 40 mm of diameter and 120 mm of height	0, 45, 90, 135, and 180
Parker and El-Genk [31]	HFE-7100	Copper (10 mm × 10 mm)	0, 60, 90, 120, 150, and 180
Kim et al. [22]	Water	Silicon wafer (20 mm × 25 mm)	0, 45, 90, 120, 135, 150, 160, and 170
Kim et al. [23]	Water	Silicon wafer (20 mm × 25 mm)	120, 135, 150, 160, and 170
Mei et al. [24]	Water	Stainless steel and Copper, 16 mm of diameter	Stainless Steel: 0, 90, 120, 150, and 180 Copper: 0, 30, 90, 150, and 180

Table 2
Correlations of the pool boiling CHF.

Reference	Correlation	Working Fluid
Vishnev [8]	$\frac{q''_{CHF}}{q''_{0^\circ}} = \frac{(190-\theta)^{0.5}}{190^{0.5}}$	Helium
El-Genk and Guo [13]	$q''_{CHF} = C_{CHF}\,\rho_g\,h_{fg}\left[\frac{\sigma(\rho_f-\rho_g)g}{\rho_g^2}\right]^{1/4}$ $C_{CHF,\,water} = 0.034 + 0.0037(180-\theta)^{0.656}$ $C_{CHF,\,nitrogen} = 0.033 + 0.0096(180-\theta)^{0.479}$ $C_{CHF,\,helium} = 0.002 + 0.0051(180-\theta)^{0.633}$	Water
Chang and You [15]	$\frac{q''_{CHF}}{q''_{0^\circ}} = 1 - 0.0012\,\theta\tan(0.414\,\theta) - 0.122\sin(0.318\,\theta)$	FC-72
Brusstar and Merte [14]	$\frac{q''_{CHF}}{q''_{0^\circ}} = \begin{cases} 1.0 & 0^\circ < \theta \leq 90 \\ (\sin\theta)^{1/2} & 90^\circ \leq \theta < 180 \end{cases}$	R113
Arik and Bar-Cohen [16]	$\frac{q''_{CHF}}{q''_{0^\circ}} = 1 - 0.001117\,\theta + 7.79401 \times 10^{-6} \times \theta^2 - 1.37678 \times 10^{-7} \times \theta^3$	HFE-7100 and FC-72
Priarone [18]	$q''_{CHF} = C_{CHF}\,f(\theta)\,\{\rho_g^{0.5}\,h_{fg}\,[g\,\sigma\,(\rho_f-\rho_g)]^{1/4}\} f(\theta) = 1 - 0.001117\,\theta + 7.79401 \times 10^{-6} \times \theta^2 - 1.37678 \times 10^{-7} \times \theta^3 C_{CHF} = 0.165\ (for\ FC-72) C_{CHF} = 0.21\ (for\ HFE-7100)$	HFE-7100 and FC-72

and zero ozone depletion potential with a wide range of boiling points and have excellent thermal stability.

Howard and Mudawar [17] conducted a pool boiling experiment with a copper block in saturated FC-72 and PF-5052. They divided the boiling process into three major regions based on the vapor behaviors, namely, upward facing($0^{\circ} \leq \theta < 60^{\circ}$), near vertical($60^{\circ} \leq \theta < 165^{\circ}$), and downward facing ($165^{\circ} \leq \theta \leq 180^{\circ}$) regions. Additionally, they proposed a pool boiling CHF correlation for the near vertical region based on the 2-D interfacial instability theory, separated flow model, energy balance, and criterion for separation of the wavy interface from the heated surface at the CHF.

Priarone [18] and Liao et al. [19] had similar observations for the CHF at various inclination angles. A slight decrease in the CHF was observed when the inclination angle was increased (0° to 90°), whereas a dramatic decrease was observed with an increasing inclination angle ($90^{\circ} < \theta \leq 180^{\circ}$). Additionally, Priarone developed a correlation for the CHF as a function of the inclination angle, as suggested by Kutateladze [20] and Zuber [21].

By observing the bubble dynamics and hydrodynamics on the silicon wafer heater, Kim et al. [22] and Kim et al. [23] found that the heater coated by graphene resulted in the early Onset of Nucleate Boiling (ONB), especially when the heater was facing downward. Moreover, by using the bare heater, the CHF was observed to be constant or slightly decreased on the graphene heater as the heater was placed at inclination angles ranging from 0° to 90° and to be sharply decreased as the heater orientation increased towards 180°.

Recently, Mei et al. [24] reported the effects of the surface orientation on the heat transfer coefficient and the CHF of nucleate boiling. They observed that CHF slightly decreased as the orientation surface increased from 0° to 120° inclination angles, and sharply decreased as the surface orientation increased towards 180°.

The above results reveal the need for a more detailed experimental study on the nucleate pool boiling and CHF at various inclination angles. The key objective of this study is to elucidate and analyze the complex processes and phenomena involved in pool boiling CHF at various inclination angles. A high-speed digital camera was used to capture the pool boiling phenomena at various inclination angles. In this study, boiling phenomena such as bubble generation, departure diameter, frequency, and nucleation sites density were observed until the CHF occurred on the heated surface.

2. Experimental methods

The experimental facility was designed to observe the complex phenomena involved in pool boiling at various inclination angles. Fig. 1 illustrates the schematic of the experimental setup. The experimental facility consisted of the test section, DC power supply SM 15-11 S223 (15 V × 100 A), current sensor input terminal, power meter (YOKOGAWA WT310E), and high-speed camera (MIRO EX4). The power supply was connected to the digital power meter by the current sensor input terminal to monitor the exact output power sent to the printed circuit board (PCB) heater. The experiments were performed for 0°, 45°, 90°, 135°, and 180° inclination angles with the test conditions summarized in Table 3.

2.1. Pool boiling test section

The pool boiling test section was made of Aluminum with a rectangular cross-section (60 × 260 mm) and a height of 160 mm. Two Polycarbonate visualization windows (125 mm × 85 mm) were held in place by laterally compressing the assembly with a set of M4 fasteners. A thin flat copper heater with the length of 100 mm, the width of 1.5 mm, and thickness of 50 μm was manufactured on the PCB as shown in Fig. 2. The PCB was mounted on the bed heater made of Acetal before it was installed at the bottom part of the pool boiling test section.

A pre-heater (100 W) and K-type sheathed thermocouple were placed 25 mm horizontally apart from the PCB heater to heat the water up to the saturation condition and to monitor the temperature, respectively. Furthermore, the pool boiling test section was covered by a stainless-steel heating jacket (250 W) to maintain the bulk temperature at saturation condition and minimize the heat loss. Another K-type thermocouple was placed on the heating jacket to monitor the temperature of the heat supplied to the test section through the heating jacket.

2.2. Experimental procedure

2.2.1. PCB heater fabrication

The PCB heater surface was polished with CC-2000Cw sandpaper prior to Alumina powder (0.3 μm) to ensure uniform and better surface conditions in every experiment. The polishing process was done with the aid of the Buehler US/METASERV 2000 grinder polisher and CHEMOMET 8 as the polish cloth. Furthermore, the polished PCB heater surface was cleaned with water prior to ethanol, blown dry with air, and oven-dried at 50 °C for at least 10 min to prevent the onset of moisture on the polished PCB heater surface. Fig. 3(b) and (c) show the polished PCB heater surface with an average roughness of ±0.1 μm as analyzed by atomic force microscopy (AFM, XE-70, Park System, Inc.) shown in Fig. 3(a). Moreover, Fig. 4 shows the hydrophilic surface of the polished PCB heater with an average static contact angle of ±81.94° as measured by the sessile drop technique [25].

2.2.2. Pool boiling experiment

The pool boiling test section was filled with deionized water and heated up to the saturation temperature by the preheater (100 W). The preheater was turned off once the bulk temperature reached the saturation temperature to avoid bubble generation on the preheater surface. When the bulk temperature was stable in the saturation condition, the heating jacket was turned on with the temperature set between 50 and 90 °C. The high-speed camera with the resolution of 800 × 600 pixels and rate of 1200 frames per second was used to record the video and photographs during the experiment to gain a more detailed understanding of the boiling phenomena. The test section was highlighted with 500 W halogen light intensity during the recording of the bubble phenomena. The video files, bulk temperature, and the power data were automatically read, converted, measured, and saved on the personal computer.

2.2.3. Image processing

The recorded images were analyzed by using Matlab to determine the bubble departure diameter. The basic image processing functions were used to process the image and detect the maximum and minimum lengths of the axes to calculate the bubble diameter as the bubble was assumed to be ellipsoidal and symmetric around the minimum axis. By knowing the maximum and minimum lengths, an equivalent ellipsoid bubble diameter was calculated using Eq. (1) [26].

$$d_b = \sqrt[3]{(d_{max})^2\,(d_{min})} \tag{1}$$

where d_{max} and d_{min} are the maximum and minimum lengths of the axes, respectively. Through the recorded images, the nucleation sites were detected. On the other hand, bubble departure frequency

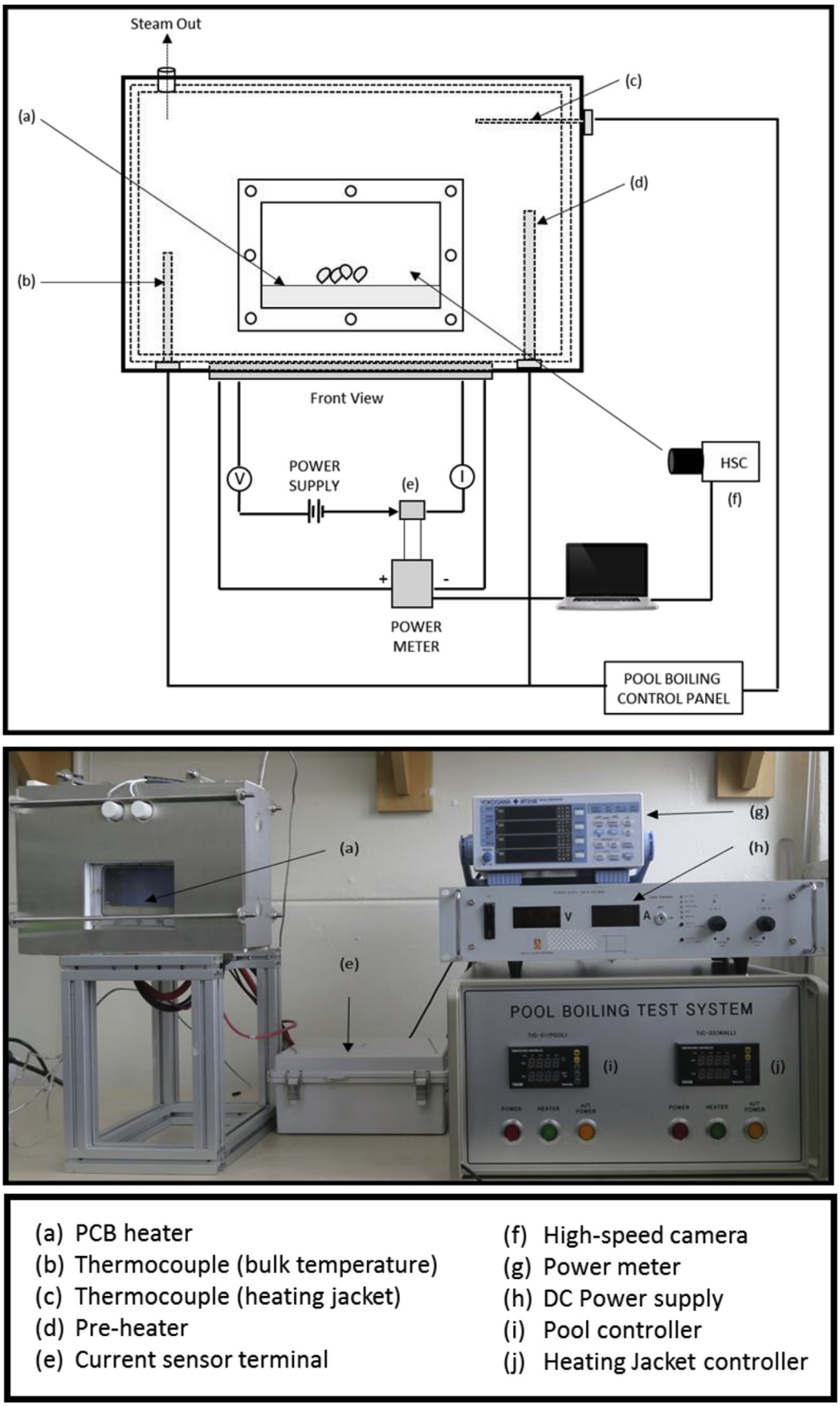

Fig. 1. Schematic diagram and image of pool boiling experimental facility.

Table 3
Test conditions.

Parameter	Value
Bulk temperature (℃)	100
Heating jacket temperature (℃)	70–90
Heat flux (MW/m^2)	0.03–1.614
PCB heater surface roughness (μm)	±0.1
PCB heater surface wettability (°)	±81.94
Inclination angle (°)	0–180

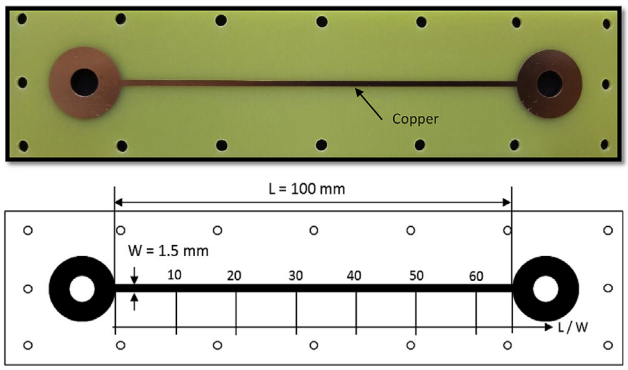

Fig. 2. Dimensions and image of the PCB heater.

was determined using the relation $f = \frac{1}{t_g + t_w}$. In this relation, t_g is the duration of the bubble growth and t_w is the bubble waiting time between the departure of each bubble and the appearance of the next generated bubble. Due to the measured bubble departure diameter and the value of bubble frequency and nucleation site are different in every image, the value of the bubble departure diameter, frequency and nucleation site density in this study constituted the average value.

2.2.4. Uncertainty analysis

The experiment was conducted several times to ensure the repeatability of the data. In this study, the data reported was statistically analyzed. The uncertainties related to the experimental parameters were analyzed. Table 4 summarized the uncertainty of the parameters; geometry (PCB heater area), measurement of the bubble parameter, inclination angle, voltage, bulk and heating jacket temperature, and the heat flux result. The heat flux supplied to the PCB heater was calculated by using the voltage signal measured by the DAQ which calibrated into power, and divided by the area of the heater. The uncertainties were approximately 0.1% and 0.05% for the voltage and the heater area, respectively. Meanwhile, the uncertainty of the heat flux was calculated by Eq. (2) proposed by Moffat [27];

$$\delta R = \sqrt{\sum_{i=1}^{n} \left(\frac{\partial R}{\partial X_i} \cdot \delta X_i \right)^2} \tag{2}$$

where δR is the uncertainty value, R is the calculation result based on the measurement, X_i is the i^{th} variable, and δX_i is the uncertainty of i^{th} variable. The uncertainty of the heat flux in this study was

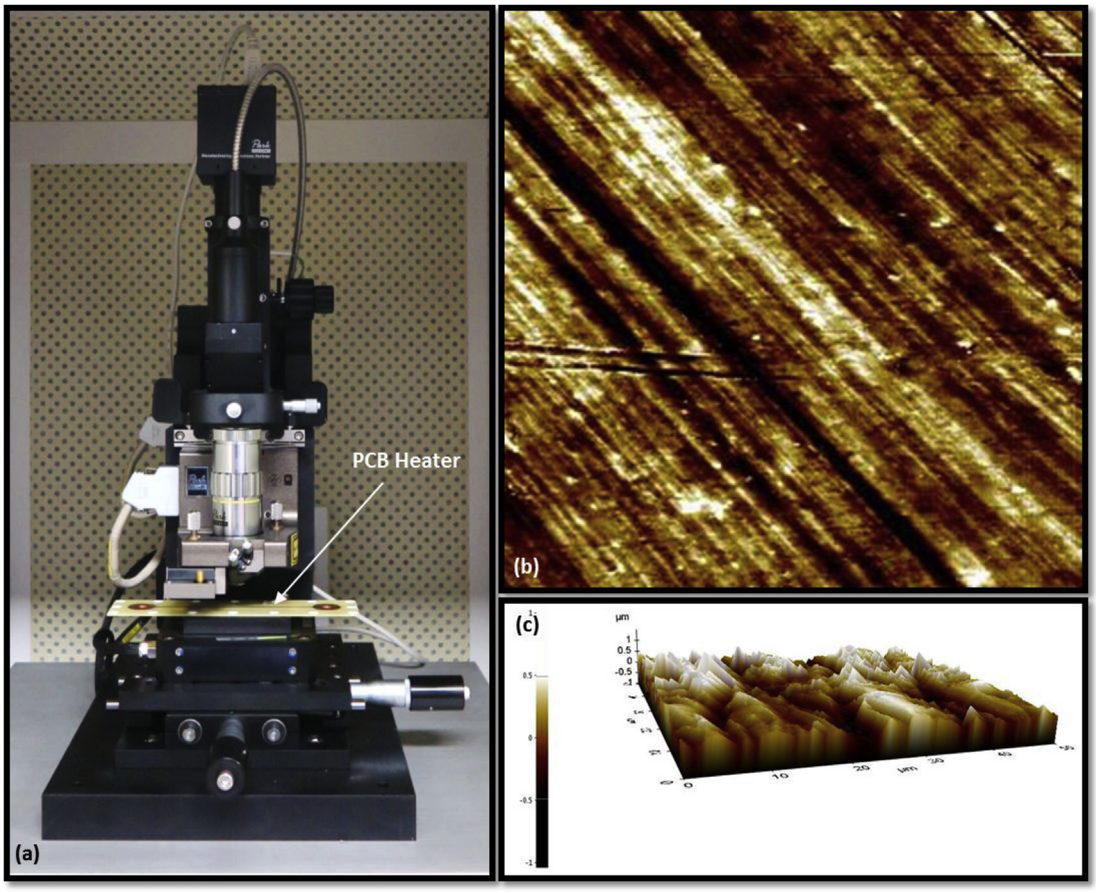

Fig. 3. Surface roughness measurement; (a) AFM machine; (b) 2-D heater surface roughness; (c) 3-D heater surface roughness.

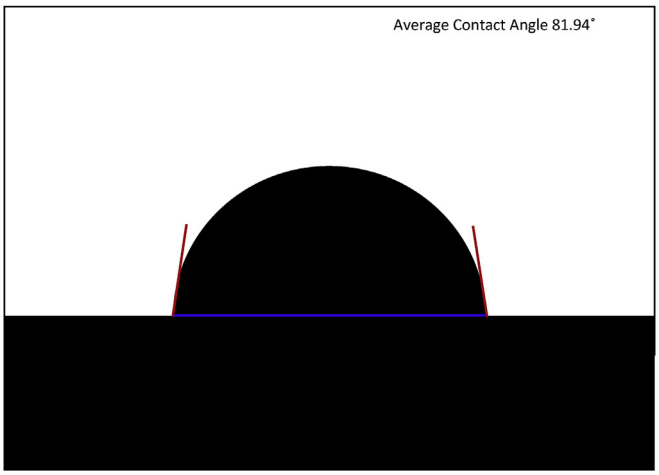

Fig. 4. Average static contact angle of a water droplet on the PCB heater surface.

Table 4
Uncertainty of the experimental parameters.

Parameter	Uncertainty
Heater area	±0.05%
Bubble departure diameter	±0.015 mm
Heater inclination angle	±1°
Voltage	±0.1%
Bulk temperature	±1 °C (0.4%)
Heating jacket temperature	±1 °C (0.4%)
Heat flux	±0.61%

estimated as 0.61%. On the other hand, the maximum uncertainties of the bulk and heating jacket temperature based on the K-type thermocouple were ±0.5% (±1 °C). As the PCB heater mounted on a bed heater and installed at the bottom part of the test section, the inclination angle was measured by measuring the incline of the test section by inclinometer with the uncertainty approximately of 1°. The basic recording speed and the image size on the camera were set at 1200 frame per second and 800 × 600 pixels, respectively. A reference size probe was installed on the test section, and the bubble size was calibrated based on the reference probe size. Based on the calculation of bubble departure diameter, the uncertainty of the calculation of bubble departure diameter was estimated 1 pixel or ±0.015 mm.

3. Results and discussion

Experimental observations of the bubble behaviors and CHF on PCB heater in saturated pool water at various inclination angles were conducted using the facilities described in the previous section. A detailed discussion of the bubble behaviors and CHF is given below.

3.1. Effect of the inclination angle on bubble phenomena

In this study, a heater placed at 0° inclination angle was used as the reference. When the condition of the wall superheat became sufficient to cause vapor nucleation at the heating surface, the first generated bubble was considered as the ONB.

Fig. 5 shows the visualization of the bubble phenomena on the PCB heater at increasing heat flux for various inclination angles.

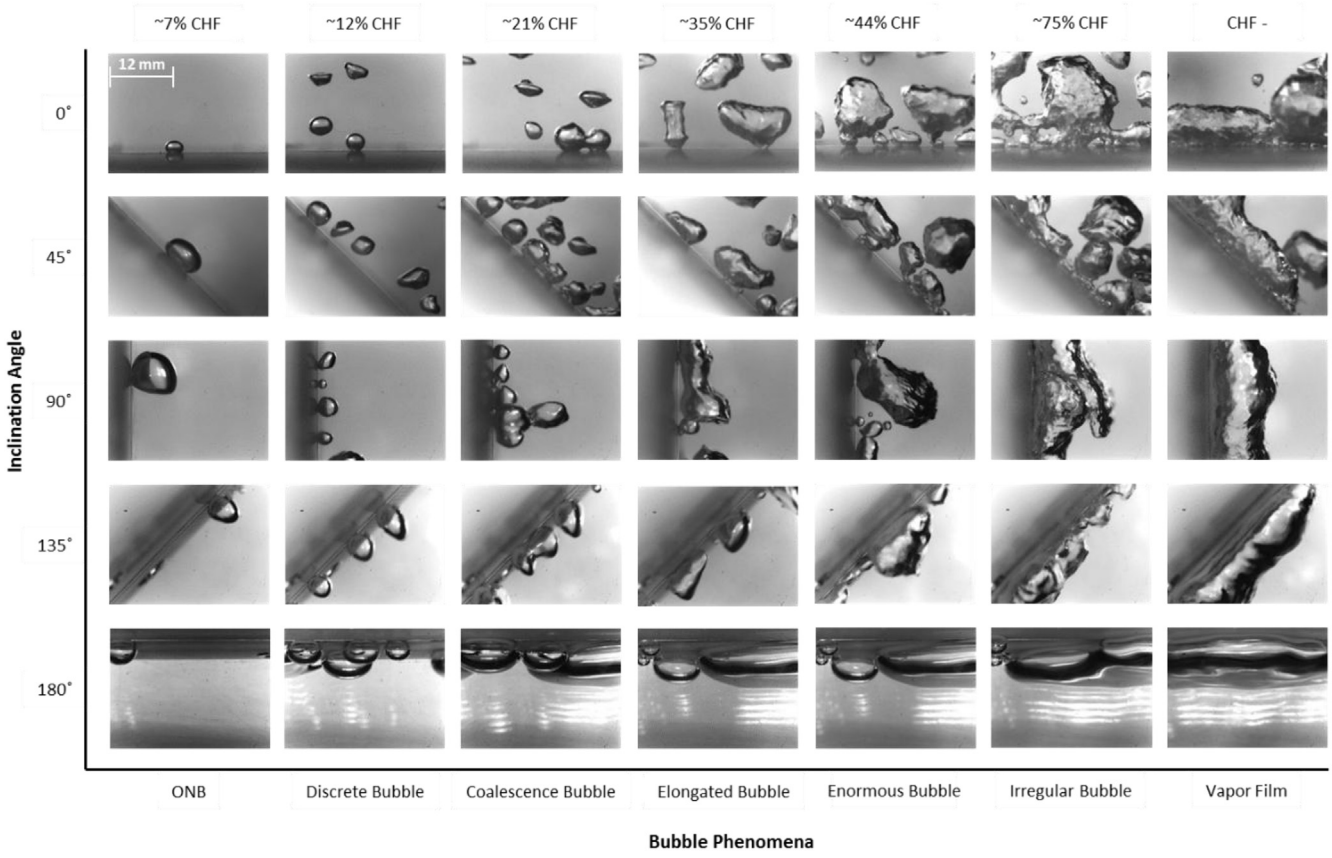

Fig. 5. Photographs of bubble phenomena in saturated pool at various inclination angles.

When the PCB heater was placed at 0° inclination angle, the ONB occurred at the exact location where the CHF occurred (at 4.9% of CHF). At a very low heat flux (9% of CHF), the water near the surface is superheated and evaporates, forming discrete bubbles wherever there are nucleation sites. The generated bubble exhibited a flattened shape transforming into spherical as it grew. Subsequently, the spherical bubble became ellipsoidal as it detached vertically from the heated surface. A further increase in the heat flux triggered an increase in the number of active nucleation site, resulting in a smaller distance between the consecutive bubbles. As heat flux increases to 20% of CHF, the generated bubbles coalesced each other and formed an elongated bubble. These elongated bubbles were observed to depart from the heated surface earlier than a single discrete bubble. An enormous bubble was formed due to the interaction between the coalesced bubbles at 44% of CHF. The enormous bubbles grew and were observed to be of irregular shape as the heat flux increased to 74% of CHF. At a very high heat flux (94% of CHF), a vapor film was formed and covered the entire heated surface. This vapor film impeded the contact between the incoming water and the heated surface resulting in the CHF at 1.61 MW/m^2.

At 45° inclination angle, the first bubble was generated at 5.9% of CHF. Several interesting behaviors were observed related to the bubble sliding phenomenon. At 10.3% of CHF, bubble behaviors could be divided into two types. First, the bubble that was generated with a diameter $\geq$2 mm grew and detached vertically in the direction of the PCB heater. Second, the bubble that was generated with a diameter <2 mm grew and slid onto the heated surface at the same time before detaching in the vertical direction of the PCB heater. Those phenomena explained the detaching forces exceeded the attaching forces when the diameter of the generated bubble is $\geq$ 2 mm. However, when the attaching forces were stronger than the detaching forces, the generated bubble would slide along the heated surface before it detached. This phenomenon differed from that of the generated bubble with a diameter of <2 mm. As the heat flux increased, the nucleation sites became active and generated smaller spherical bubbles. The nucleation sites that were close to each other caused the generated bubbles to coalesce at approximately 20.4% of CHF. The coalesced bubbles were also formed from the contiguous bubbles successively generated on the heated surface. Elongated bubbles were formed as the result of the interaction between the coalesced bubbles when the heat supplied to the surface increased. At higher heat flux (40.7% of CHF), it was observed that the elongated bubble transformed into a huge bubble. Huge bubble with an irregular shape was formed as the heat flux increased to 66.1% of CHF before it formed a vapor film (at 82.8% of CHF). The agitation of the fluid resulted in the unstable formation of the vapor film. Finally, when the supply of fluid to the heated surface was impeded, CHF occurred at 1.41 MW/m^2.

With the PCB heater placed vertically at a 90° inclination angle, the ONB occurred at 6.91% of CHF. It showed a higher heat flux was needed to generate a bubble compared to the two previous inclination angles. The generated bubble drifted along the surface before it detached at some point because of the buoyancy. As the heat flux increased, the nucleation sites became active and generated tiny bubbles. An elongated bubble was formed due to the bubbles generated successively on the heated surface. The elongated bubble was also formed because of the merging and coalescence bubbles while drifting along the surface. A further increase in the heat flux (75.5% of CHF) led the elongated bubble to interact and form a wavy vapor film. The wavy vapor film initiated and grew as they drifted upward along the surface, continuously. The agitation occurred when the wavy vapor film detached as it grew thicker and a short wetting occurred on the heated surface. The heated surface was intermittently wetted and continuous vapor film is reestablished to cover the entire heated surface. The CHF occurred at 1.28 MW/m^2 when the wavy vapor prevented the liquid to rewetting the heated surface.

Various interesting phenomena took place when the heater was placed facing downward at 135° inclination angle. Early ONB occurred at 2.27% of CHF. The generated bubble was formed in an ovoid shape and drifted along the heated surface before it detaches at the most upper part of the PCB. It showed that the attaching forces of the bubble were stronger than the detaching forces. As the heat flux increased to 8.7% of CHF, the nucleation sites on the heated surface became active and generated discrete bubbles with the same shape. By increasing the heat flux to 15.8% of CHF, discrete bubbles were generated with a smaller distance between each other. Those bubbles coalesced as they traveled along the surface. An enormous bubble was formed as the result of the continuous interaction between the coalesced and elongated bubbles at 31.7% of CHF. When the heat flux was above 60% of the CHF, the interaction between the enormous bubbles became unstable, leading to the formation of the bubble with irregular shapes. A wavy vapor initiated and drifted along the upper wall when the heat flux reached approximately 65% of CHF. This vapor film grew and laminated the heated surface to have direct contact with the liquid. Consequently, preventing the liquid to rewet the heated surface, resulting in CHF at 1.12 MW/m^2.

When the heater was placed horizontally facing downward (at 180° inclination angle), the generated bubbles grew and coalesced with each other until ultimately covering the entire heated surface. Early CHF occurred (at 0.22 MW/m^2) as a consequence of the vapor film laminating the entire surface, hindering the liquid supply to reach the heated surface.

3.2. Effect of the inclination angle on the boiling curve

The boiling curve at various inclination angle was demonstrated in Fig. 6. As shown in Fig. 6, the ONB heat flux increased with increasing surface orientation (0° to 90° inclination angles). The phenomena changed when the heater placed facing downwards (at 135° and 180° inclination angles), early ONB occurred due to the boundary layer of the natural convection is thicker. This observation is similar to Kim et al. [22] and Jung et al. [28], early ONB occurred in the case of the downward facing heater.

The unstable pattern on the boiling curve was observed at low heat flux (1–21% of CHF) and became stable as the heat flux increased above the 21% of CHF. The stable pattern on the boiling curve shows a reduction of CHF by increasing inclination angle (from 0° to 180°) as also reported by previous studies [7,15,17,18]. The occurrence of CHF indicated the end of nucleate boiling. As shown in Fig. 6, the larger angle has the lowest value of CHF. Bubbles that were generated from the surface horizontal and facing upwards detached easily. As a result, the detached bubbles provided free space inside the cavities allowing the fluid to rewet the surface to delay the CHF. On the other hand, bubbles that were generated from the surface facing downwards will coalesce and cover the heated surface, precluding the liquid to rewet the surface.

3.3. Effect of the inclination angle on CHF

The CHF occurred at very high heat flux when the vapor film laminated the surface and prevented the liquid from reaching the heated surface. Fig. 7 compares the CHF value in this study with the prediction of existing correlation by El-Genk and Guo [13] for water as the working fluid. The present data showed consistency with the similar trend. The CHF decreased as the heater orientation increased from 0° to 180° inclination angles. Higher CHF value in this study possibly due to the different experimental method, heater properties, working fluid, thickness, roughness, size, and

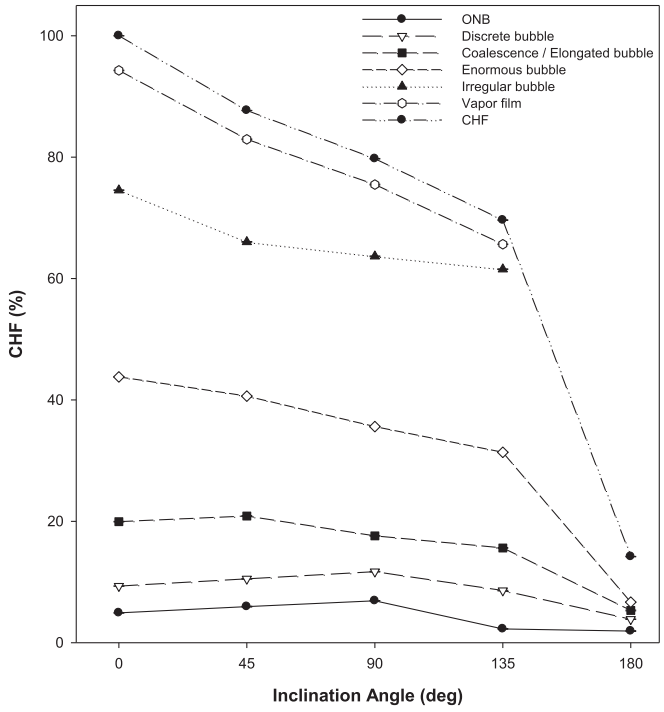

Fig. 6. Boiling curve at various inclination angles.

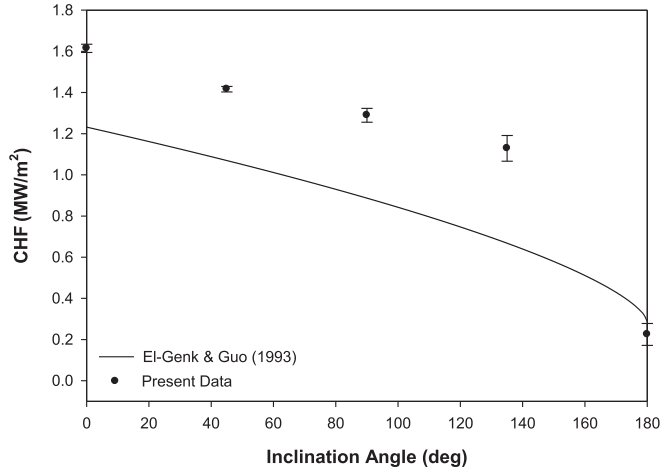

Fig. 7. Comparison of existing CHF data with the correlations of pool boiling CHF at various inclination angles with the same working fluid (water).

geometry of the heater. Among those differences, the heater size and geometry were the main causes of higher CHF values, as mentioned in section 1.

Fig. 8 compares the normalized CHF of the present study with the CHF predicted from the correlations summarized in Table 2. The normalized values in Fig. 8 showed the ratio of the CHF and CHF_{max} (at 0° inclination angle). The CHF ratio in the present study shows a similar trend with those CHF ratios calculated by the correlations in Table 2. The CHF decreased with increasing the inclination angle (from 0° to 180°). However, as discussed earlier, CHF was also affected by some differences (working fluid, heater size and geometry). As a result, the different in CHF ratio between this study and their studies [8,13–16,18] is approximately 13–50%.

Fig. 9 illustrates the CHF location by the ratio of the length (L) and width (W) of the PCB heater at inclined surfaces. The detailed dimension of PCB heater with the ratio of L/W is provided in Fig. 2.

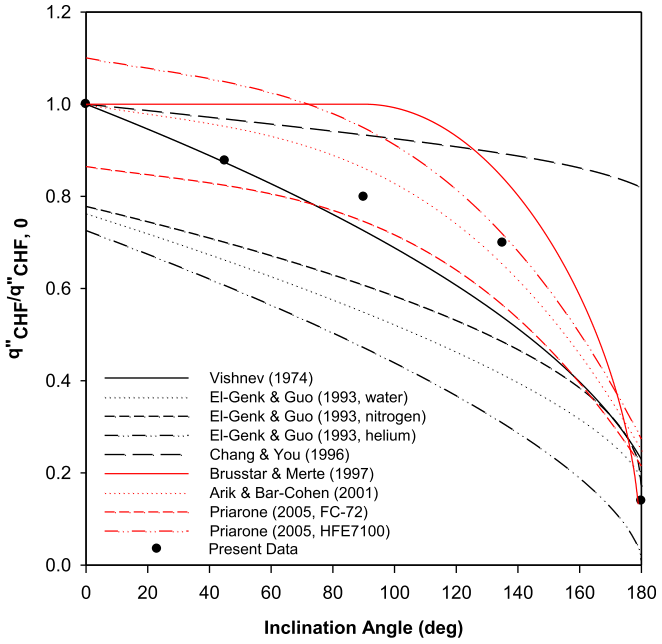

Fig. 8. Normalization of CHF at various inclination angles.

When the heater placed horizontally (at 0° and 180° inclination angles), the CHF occurred at the exact location where the first bubble generated. As the PCB heater inclined at a 45° angle, CHF occurred at L/W = 41.10 due to the contiguous vapor slid upward for some distance before it detaches easily in a vertical direction of the heated surface. When the heater placed vertically (at 90° inclination angle), the CHF occurred at the upper side of the heated surface (L/W = 63.53) due to the vapor film behaviors. The vapor film grew as they slid along the upper surface causing the vapor film at the upper side to be thicker than the lower side. When the heater placed facing downward (at 135° inclination angle), the CHF occurred at L/W = 56.13 due to the vapor film was trapped and could not detach easily from the heated surface.

3.4. Effect of the inclination angle on bubble departure diameter, frequency, and nucleation site density

The image processing by Matlab was used to analyze

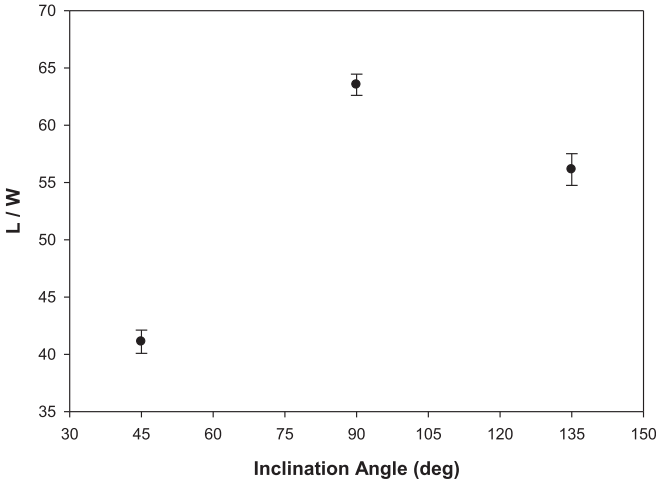

Fig. 9. Location of CHF on the PCB heater at inclined surfaces.

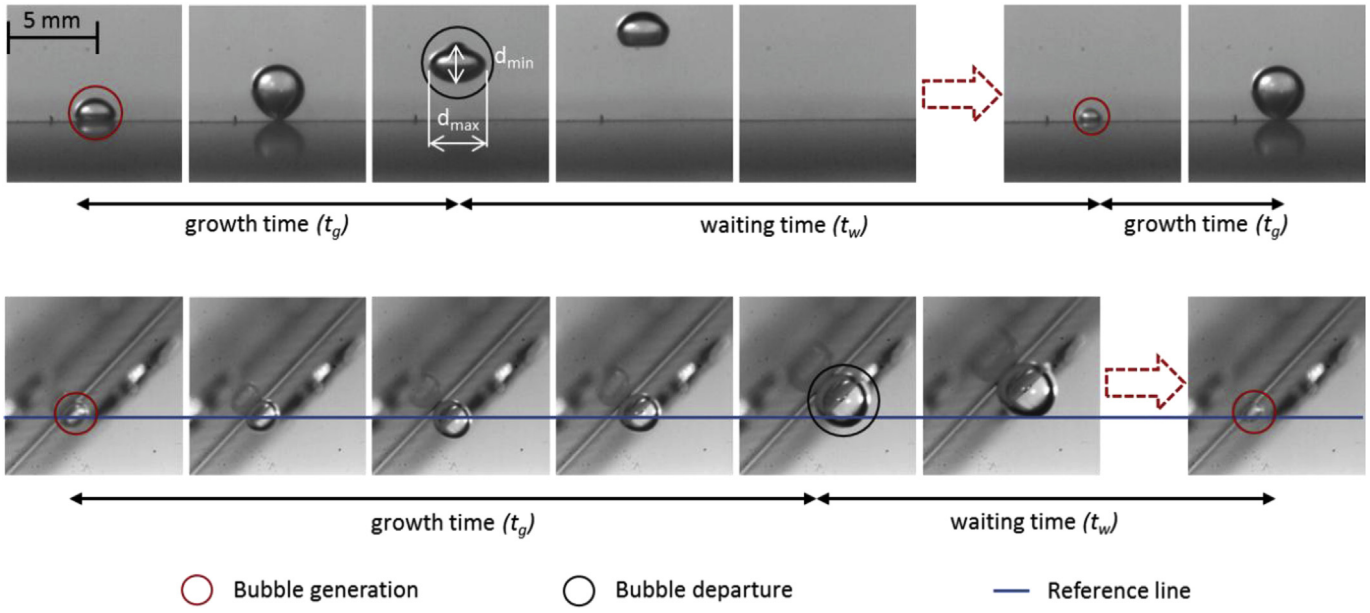

Fig. 10. Bubble departure diameter, growth, and waiting time according to the heater inclination angle.

approximately 10,000 images from the experimental data. The bubble departure diameters at 0° and 45° inclination angles were measured when the first bubble generated (ONB) and detached vertically from the heated surface. On the other hand, at 90° and 135° inclination angles, the first generated bubble (ONB) that drifted on the heated surface was considered as the departed bubble. Fig. 10 illustrates the bubble departure diameter, growth, and waiting time according to the heater inclination angle. In this study, the bubble departure diameter at a 180° inclination angle was not measured as it could not be observed due to the bubble behavior at this condition. Fig. 11 displays the comparison of the bubble departure diameter with the experimental data of Jung and Kim [29]. The bubble departure diameter increased when the heater was placed at 0° to 90° inclination angles and decreased when it was placed at 135° inclination angle. Jung and Kim [29] had made a similar observation, finding that the bubble departure diameter increased with increasing surface orientation from 0° to 60° inclination angles and increased dramatically at a 90° inclination angle. In their study, 700 nm thick rectangular indium-tin-oxide (ITO) film with the dimensions of 8 mm by 15 mm was used as the heater. They compared the bubble departure diameter for various inclination angles at constant wall superheat. At a 90° inclination angle, the bubble diameter was measured at the partial boiling zone after the ONB with a higher heat flux. Consequently, the bubble departure diameter at this angle was the highest among all the inclination angles. Kim et al. [30] reported based on their visualization observation that the approximate bubble size on the heater facing upwards were bigger compared to those with the heater placed facing downwards, which is similar to the observation in this study. This happened as the bubbles on the heater facing upward freely departed from the heated surface by buoyancy. Meanwhile, the generated bubbles on downward facing heater were forced to drift upward and could not depart easily from the heated surface because of the presence of the surface.

Bubble frequency is the number of generated bubbles from a nucleation site per unit of time. As explained in Section 2.2.3, the bubble departure frequency was determined by using the period as the total of the time (bubble growth and waiting time), as

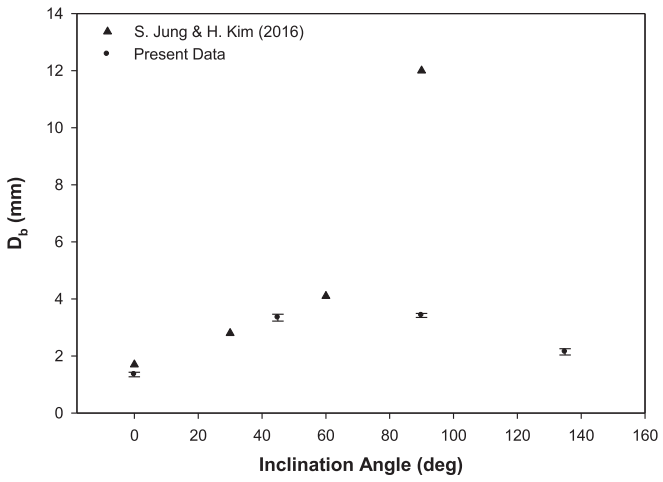

Fig. 11. Bubble departure diameter at various inclination angle.

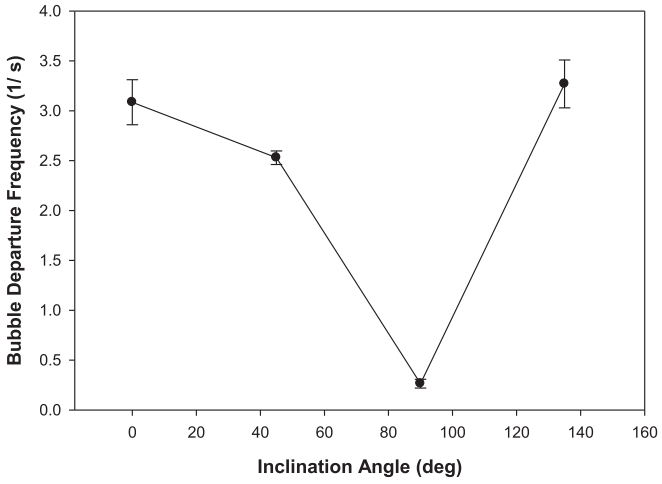

Fig. 12. Effect of heater surface orientation on bubble departure frequency.

Table 5
Bubble parameters at various inclination angles.

Inclination Angle (deg)	Bubble Departure Diameter (mm)	Bubble Departure Frequency (1/s)	Nucleation Site Density (#/mm^2)	
			q'' = 0.25 MW/mm^2	q'' = 0.30 MW/mm^2
0	1.35	3.08	0.34	0.41
45	3.34	2.52	0.41	0.50
90	3.42	0.26	0.67	0.79
135	2.14	3.26	0.33	0.39

illustrated in Fig. 10. The bubble departure frequency on the PCB heater at various inclination angles is depicted in Fig. 12. Bubble departure frequency at 90° inclination angle was the lowest among the other four inclination angles. It was also observed that to generate a big bubble as measured at 90° inclination angle required a longer time. The bubble departure diameters, frequencies, and waiting times in this study are summarized in Table 5.

Moreover, based on the high-speed visualization, the increasing heater surface orientation from 0° to 90° inclination angles attributed to an increased number of active nucleation sites. However, at 135° inclination angles, it was observed that the number of active nucleation sites reduced. Fig. 13 shows the number of active nucleation site at various inclination angle with increasing heat flux. The active nucleation site increased with the increase of heat flux. In this study, certain heat fluxes (0.25 and 0.3 MW/m^2) were selected to observe the effect of surface orientation on nucleation site density as illustrated in Fig. 14. The result is consistent with the previous studies [15,29], the number of active nucleation site increased with increasing surface orientation from 0° to 90° as the result of better heat transfer at the higher inclination angles.

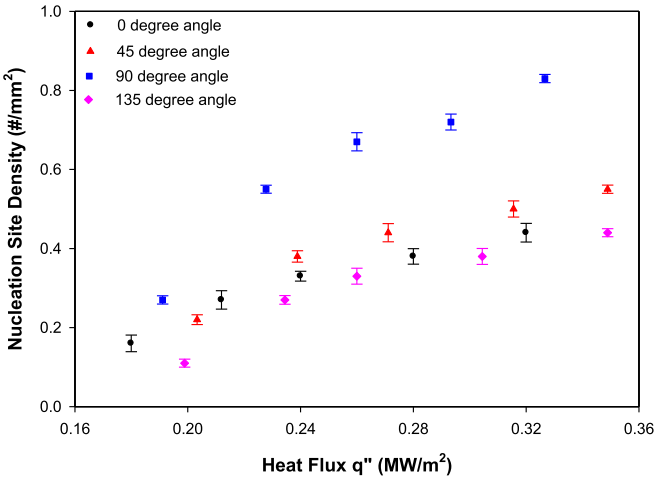

Fig. 13. Nucleation site density with increasing heat flux at various inclination angles.

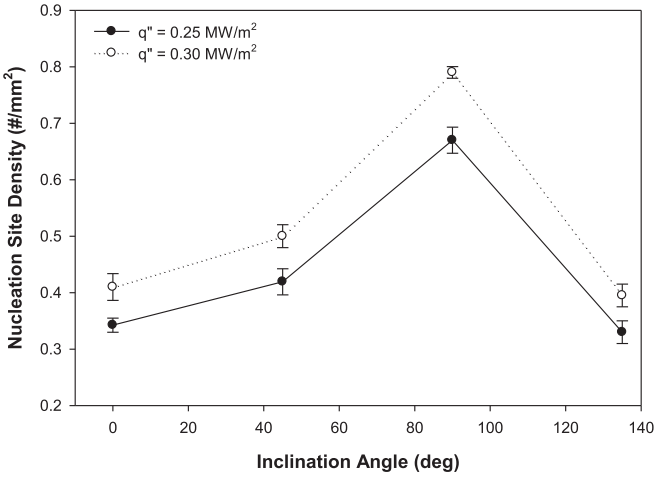

Fig. 14. Nucleation site density for certain heat flux at various inclination angles.

4. Conclusions

Experimental studies of the bubble behaviors and CHF on a PCB in a saturated water pool at various inclination angles were conducted. With the heater surface placed at 0°, 45°, 90°, 135°, and 180° inclination angles, the primary findings of this study are summarized below:

- Higher heat flux was needed to reach a certain temperature to generate bubbles on the heated surface when the heater was placed at 45° and 90° inclination angles. However, when the heater was placed facing downward at 135° and 180° inclination angles, the boundary layer of the natural convection became thicker, resulting in the early ONB.
- Based on the investigation in this study, at partial boiling (low heat flux), the bubble behaviors became unstable. The behaviors showed stability when the heat flux was above 21% of the CHF and showed typical boiling behaviors.
- The phenomena at the vertical position of the heater surface were the most remarkable, as the 90° inclination angle had the highest ONB heat flux, biggest bubble departure diameter, the longest bubble waiting time, highest number of active nucleation site, and lowest bubble frequency among the other four inclination angles.
- At 0° and 45° inclination angles, the bubbles generated and detached in the vertical direction of the heated surface. At a 45° inclination angle, the generated bubble grew and slid for some distance before it detaches from the surface. At 90° and 135° inclination angles, the bubbles formed and drifted upward along the heated surface. However, at a 180° inclination angle, the generated bubbles coalesced with each other. Early CHF occurred as the heated surface was laminated by the coalesced bubble and hindered the direct contact between the heated surface and the liquid.
- The inclination angle affected the CHF limit obviously. As the inclination angle increased, the limit of the CHF reduced.

Acknowledgement

This work was supported by the National Research Foundation of Korea grant funded by the Korean government (NRF-2016M2B2A9A02944795)

References

[1] S.M. Kwark, et al., Effectsf of pressure, orientation, and heater size on pool boiling of water with nanocoated heaters, Int. J. Heat Mass Tran. 53 (23–24)

(2010) 5199–5208.
[2] K. Rainey, S. You, Effects of heater size and orientation on pool boiling heat transfer from microporous coated surfaces, Int. J. Heat Mass Tran. 44 (14) (2001) 2589–2599.
[3] M.-C. Lu, et al., Critical heat flux of pool boiling on Si nanowire array-coated surfaces, Int. J. Heat Mass Tran. 54 (25) (2011) 5359–5367.
[4] K.-H. Chu, R. Enright, E.N. Wang, Structured surfaces for enhanced pool boiling heat transfer, Appl. Phys. Lett. 100 (24) (2012) 241603.
[5] P. Githinji, R. Sabersky, Some effects of the orientation of the heating surface in nucleate boiling, J. Heat Tran. 85 (4) (1963), 379–379.
[6] B.D. Marcus, D. Dropkin, The effect of surface configuration on nucleate boiling heat transfer, Int. J. Heat Mass Tran. 6 (9) (1963) 863–866.
[7] N. Kaneyasu, et al., Effect of surface configuration on nucleate boiling heat transfer, Int. J. Heat Mass Tran. 27 (9) (1984) 1559–1571.
[8] I. Vishnev, Effect of orienting the hot surface with respect to the gravitational field on the critical nucleate boiling of a liquid, J. Eng. Phys. Thermophys. 24 (1) (1973) 43–48.
[9] D. Lyon, Boiling heat transfer and peak nucleate boiling fluxes in saturated liquid helium between the/lambda/and critical temperatures, Intern. Advan. Cryog. Eng (1965) 10.
[10] L.-T. Chen, Heat transfer to pool-boiling Freon from inclined heating plate, Lett. Heat Mass Tran. 5 (2) (1978) 111–120.
[11] W.M. Rohsenow, A Method of Correlating Heat Transfer Data for Surface Boiling of Liquids, Mass.: MIT Division of Industrial Cooporation, Cambridge, 1951 [1951].
[12] Z. Guo, M.S. El-Genk, An experimental study of saturated pool boiling from downward facing and inclined surfaces, Int. J. Heat Mass Tran. 35 (9) (1992) 2109–2117.
[13] M.S. El-Genk, Z. Guo, Transient boiling from inclined and downward-facing surfaces in a saturated pool, Int. J. Refrig. 16 (6) (1993) 414–422.
[14] M.J. Brusstar, H. Merte, Effects of heater surface orientation on the critical heat flux—II. A model for pool and forced convection subcooled boiling, Int. J. Heat Mass Tran. 40 (17) (1997) 4021–4030.
[15] J. Chang, S. You, Heater orientation effects on pool boiling of micro-porous-enhanced surfaces in saturated FC-72, J. Heat Tran. 118 (4) (1996) 937–943.
[16] M. Arik, A. Bar-Cohen, Ebullient cooling of integrated circuits by novec fluids, in: Proc. Pacific Rim Int. Intersociety, Electronic Packaging Conference(IPACK'01), Kauai, Hawaii, July 8-13, 2001.
[17] A.H. Howard, I. Mudawar, Orientation effects on pool boiling critical heat flux (CHF) and modeling of CHF for near-vertical surfaces, Int. J. Heat Mass Tran. 42 (9) (1999) 1665–1688.
[18] A. Priarone, Effect of surface orientation on nucleate boiling and critical heat flux of dielectric fluids, Int. J. Therm. Sci. 44 (9) (2005) 822–831.
[19] L. Liao, R. Bao, Z. Liu, Compositive effects of orientation and contact angle on critical heat flux in pool boiling of water, Heat Mass Tran. 44 (12) (2008) 1447–1453.
[20] S.S. Kutateladze, Boiling heat transfer, Int. J. Heat Mass Tran. 4 (1961) 31–45.
[21] N. Zuber, Hydrodynamic Aspects of Boiling Heat Transfer (Thesis), Ramo-Wooldridge Corp, Los Angeles, CA (United States), 1959. Univ. of California, Los Angeles, CA (United States).
[22] T. Kim, et al., Orientation effects on bubble dynamics and nucleate pool boiling heat transfer of graphene-modified surface, Int. J. Heat Mass Tran. 108 (2017) 1393–1405.
[23] J.M. Kim, J.H. Kim, H.S. Ahn, Hydrodynamics of nucleate boiling on downward surface with various orientation. Part I: departure diameter, frequency, and escape speed of the slug, Int. J. Heat Mass Tran. (2017).
[24] Y. Mei, et al., Effects of heater material and surface orientation on heat transfer coefficient and critical heat flux of nucleate boiling, in: 2017 25th International Conference on Nuclear Engineering, American Society of Mechanical Engineers, 2017.
[25] Hai Trieu Phan, N. Caney, Philippe Marty, Stéphane Colasson, Jérôme Gavillet, Surface wettability control by nanocoating: the effects on pool boiling heat transfer and nucleation mechanism, Int. J. Heat Mass Tran. 52 (2009) 13.
[26] A. Couvert, M. Roustan, P. Chatellier, Two-phase hydrodynamic study of a rectangular air-lift loop reactor with an internal baffle, Chem. Eng. Sci. 54 (21) (1999) 5245–5252.
[27] R.J. Moffat, Describing the uncertainties in experimental results, Exp. Therm. Fluid Sci. 1 (1) (1988) 3–17.
[28] J. Kim, et al., Experimental study of heating surface angle effects on single bubble growth, J. Mech. Sci. Technol. 20 (11) (2006) 1980–1992.
[29] S. Jung, H. Kim, Effects of surface orientation on nucleate boiling heat transfer in a pool of water under atmospheric pressure, Nucl. Eng. Des. 305 (2016) 347–358.
[30] K. JJ, et al., Boiling Visualization and Critical Heat Flux Phenomena in Narrow Rectangular Gap, Idaho National Lab. (United States). Funding organisation: US Department of Energy, United States, 2004.
[31] J.L. Parker, M.S. El-Genk, Saturation and subcooled boiling of HFE-7100 on pinned surfaces at different orientations, Ratio 8 (2009) 8.